Available online at www.sciencedirect.com

SciVerse ScienceDirect

Scripta Materialia 65 (2011) 1010–1013

Scripta MATERIALIA

www.elsevier.com/locate/scriptamat

Ductile crack initiation and propagation assessed via in situ synchrotron radiation-computed laminography

T.F. Morgeneyer,[a,*] L. Helfen,[b,d] I. Sinclair,[c] H. Proudhon,[a] F. Xu[b] and T. Baumbach[b]

[a] *Mines ParisTech, Centre des Matériaux, CNRS UMR 7633, BP87 91003 Evry cedex, France*
[b] *ANKA/Institute for Synchrotron Radiation, Karlsruhe Institute of Technology (KIT), D-76131 Karlsruhe, Germany*
[c] *Materials Research Group, School of Engineering Sciences, University of Southampton, Southampton SO17 1BJ, UK*
[d] *European Synchrotron Radiation Facility (ESRF), BP 220, F-38043 Grenoble cedex, France*

Received 19 August 2011; revised 31 August 2011; accepted 1 September 2011
Available online 8 September 2011

Ductile crack initiation and propagation within a naturally aged aluminium alloy sheet has been observed in situ via synchrotron radiation-computed laminography, a technique specifically adapted to three-dimensional imaging of thin objects that are laterally extended. Voids and intermetallic particles, and their subsequent evolution during ductile crack extension at different associated levels of stress triaxiality, were clearly observed within fracture coupons of a reasonable engineering length-scale, overcoming the conventional sample size limitation of computed tomography at high resolutions.

Keywords: In situ laminography; Synchrotron radiation; Aluminium; Ductile fracture; Void growth

Prior porosity and brittle intermetallic phases are widely established as critical to the damage tolerance characteristics of most structural engineering alloys [1]. Historically two-dimensional (2D) techniques have been used to assess damage evolution [2]. However, this implies that on the one hand only the surface can be observed in situ, where a plane stress condition of necessity applies and, as a consequence, damage mechanisms are fundamentally different to those that may apply within the material bulk. On the other hand, if an attempt is made with classical techniques to assess damage mechanisms within a material, 2D observation techniques are destructive and in situ failure observations are not possible. Damage evolution has successfully been observed in situ in 3D via synchrotron radiation-computed tomography (SRCT), typically using specimens with a cross-section of up to a few square millimeters [3,4], and valuable data about damage mechanisms have been gained. However, plastic zone sizes and stress triaxiality levels [5,6] are not representative of the sustained macroscopic crack extension associated with many key engineering failure situations. In Refs. [6,7] arrested cracks were cut into 1 mm^2 cross-section samples and the crack tip region observed via SRCT, yielding unprecedented insights into ductile crack extension mechanisms. However, the evolution of the damage could not be observed in situ.

With recent developments in synchrotron radiation-computed laminography (SRCL), it has become possible to perform 3D imaging on objects that are extended in two dimensions but comparable to the field of view of the detector in the third direction, i.e. the supporting sheet or plate-like sample geometries. Originally developed for microsystem device inspection [8], this provides a unique opportunity to observe internal damage mechanisms in three dimensions during extended crack propagation in sheet materials [9]. In Ref. [10] fracture mechanisms in 1 mm thick carbon fibre–epoxy laminates provided insights into delamination processes via the stepwise in situ loading of a notched sample. SRCL is applied in the present study to assess ductile fracture initiation and propagation in a ductile 2XXX alloy for aerospace applications.

SRCL [11] is fundamentally similar to SRCT in a sense that objects can be imaged in three dimensions by acquisition of projection data and subsequent 3D volume reconstruction. While SRCT is especially adapted to compact or one-dimensionally elongated objects which stay in the field of view of the detector sys-

* Corresponding author. Tel.: +33 160763061; fax: +33 160763150; e-mail: thilo.morgeneyer@mines-paristech.fr

1359-6462/$ - see front matter © 2011 Acta Materialia Inc. Published by Elsevier Ltd. All rights reserved.
doi:10.1016/j.scriptamat.2011.09.005

tem under rotation, SRCL is optimized to image regions of interest (ROIs) out of flat, extended (i.e. plate-like) specimens. For this, the specimen rotation axis is inclined at an angle of $\theta < 90°$ with respect to the beam direction (where $\theta = 90°$ corresponds to the case of CT). For plate-like specimens, this enables a relatively constant average X-ray transmission over the entire scanning range of 360°, which allows reliable projection data to be acquired. Using a filtered back-projection algorithm [12], a 3D image of the ROI of the specimen around the rotation axis can be reconstructed from the 2D projections. Although the 3D Fourier domain of the specimen is not sampled completely [11], which leads to imaging artefacts, these artefacts are often less disruptive than the ones produced by (limited-angle) CT [12]. Exploiting propagation-based phase-contrast imaging [13], new applications related to weakly absorbing/weakly contrasted structures can be addressed [9,14,15].

Imaging was performed on the KIT's laminography instrument installed at beamline ID19 at the ESRF. We used an axis inclination angle of around 25° ($\theta \approx 65°$) and a monochromatic beam of 25 keV X-ray energy. Volumes were reconstructed from 1500 angularly equidistant radiographs; the exposure time of each projection was 250 ms. The scanned ROI was $\sim$1 mm^3, with a voxel size of 0.7 μm. The minimum specimen to detector distance was 70 mm, leading to relatively strong edge enhancement [13] due to the phase contrast. For 3D void representation, a simple grey value threshold was used to segment voids; a VTK software rendering routine was used to register the 3D datasets and produce the 3D images.

For the experiment, a commercial ductile 2139 Al–Cu alloy in naturally aged T3 condition for aerospace application was machined symmetrically from 3.2 to 1 mm thickness in the short-transverse (S) direction. Testing was performed in the T (long transverse)–L (rolling direction) configuration. The material has an initial void volume fraction of $\sim$0.3%: further details on the material properties are given in Refs. [6,7].

The sample geometry shown in Figure 1a was used. The notch was machined via electron discharge (EDMC) machining, resulting in a notch radius close to the EDMC wire radius of 0.15 mm. The loading was achieved via a two-screw displacement-controlled wedging device that controls the specimen crack mouth opening displacement (CMOD) similar to the one used in Ref. [10] (see Fig. 1).

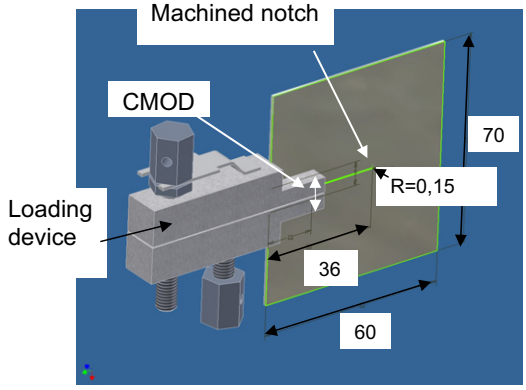

Figure 1. In situ loading device and 1 mm thick notched sample.

An anti-buckling device was used to prevent the sample from significant buckling and out-of-plane motion. The entire rig was mounted in a dedicated plate that was removed from the SRCL rotation stage between loading steps. The loading was applied via stepwise increases in the CMOD. A scan was performed before every loading step. The scanned ROIs were moved along with the propagating crack tip to image the damaged material ahead of the notch/crack tip. Twenty scans were carried out, but only the results from six of them are shown here. The video files associated with this work contain Supplementary data.

Reconstructed 2D laminography sections in the sheet plane at about the mid-thickness of the sample are shown in Figure 2a–f at different loading stages. Figure 2a shows the as-received material. The aluminium matrix is shown in grey and the initial porosities can be seen in black, with white phase contrast fringes around them. The intermetallics are seen in white. The round machined notch can be seen at the left of the sample. The features can be seen in similar quality as in tomography observations of aluminium alloys [7]. Some laminography artefacts (cf. Ref. [16]) can be seen. They do not, however, influence the segmentation of the voids/damage.

In the following are observations of ductile fracture mechanisms that have been discussed in the past but that are now seen in much greater detail via SRCL, which provides unprecedented opportunities for quantification.

Figure 2b is taken from a scan at a CMOD of 1.625 mm. About 50 μm ahead of the notch, two initial void particle clusters can be seen that have substantially evolved in size after particle fracture. The coalescence of the two voids via a narrow region of void sheeting and microvoid nucleation is observed. The coalescence does not occur via void impingement but via a shear mechanism. The shear band is evident even though the stress triaxiality is expected to be at a maximum at crack initiation at the mid-thickness, and should therefore favour void growth. The appearance of a shear coalescence band may also be linked to the void distribution, which is at almost 45° with respect to the loading direction and which may favour shear coalescence compared to impingement [17]. Similar crack bifurcation has also been observed in Ref. [18], and has been attributed to shear stresses in the vicinity of round notches. It can also be seen that the fracture starts from within the material bulk, not from the notch surface, which may be linked to a stress triaxiality maximum somewhat ahead of the notch [19]. In Figure 2c the coalescence of the two voids with the notch is observed. In Figure 2d the crack progresses and substantial void growth occurs ahead of the crack. In Figure 2e and f the crack propagates, but the void fraction ahead of the crack seems to be lower than at initiation (Fig. 2a–c).

SRCL makes it possible to visualize the voids in three dimensions, as shown in Figure 3a–c, where voids are shown in a 140 μm thick slice around the mid-thickness at different CMODs. Figure 3a shows the as-received material, with voids aligned in the L direction. At

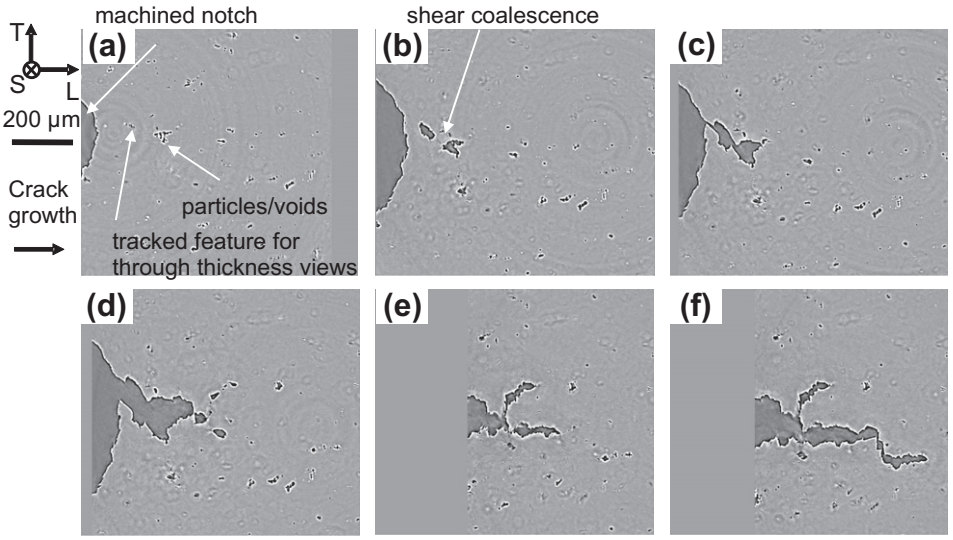

Figure 2. 2D sections at the mid-thickness of the aluminium sheet plane of reconstructed laminography data of ductile crack initiation and propagation at CMODs. (a) As-received material; (b) CMOD = 1.625 mm; (c) CMOD = 1.875 mm; (d) CMOD = 2.0625 mm; (e) CMOD = 2.3125 mm; (f) CMOD = 2.375 mm. Information on the supplementary loading steps is given in video 1.

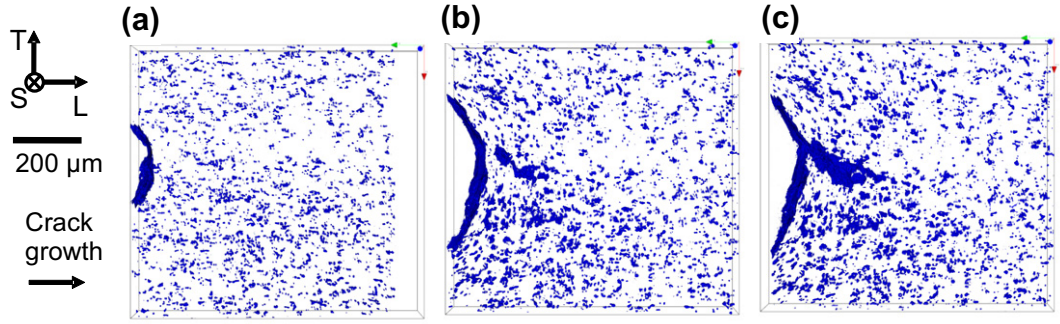

Figure 3. 3D volumes (140 µm thick slice) showing only voids and the notch around the sample's midplane for CMODs. (a) As-received material; (b) CMOD = 1.625 mm; (c) CMOD = 1.875 mm. Information on the supplementary loading steps is given in video 2.

CMOD = 1.625 mm the two large coalesced voids can again be seen. This view confirms that damage does not start immediately from the notch but ahead of it. It can also be seen that the voids around the notch are oriented tangentially to the notch circumference after large plastic deformation. The voids immediately ahead of the crack are smaller than at crack initiation (more views are shown in 3D video 2).

Figure 4a–d shows reconstructed 2D sections of the material in the through-thickness (T–S) plane. This plane was chosen with regard to the feature indicated in Figure 2a that is followed for all sections. The necking of the material can be discerned. Differences in void growth can be seen between the sample's middle and its edges. The zone in which void growth is observed is extended to over ~600 µm in height. It can be seen in Figure 3c that the crack centre does not cover the entire sheet thickness as it forms a triangle and/or tunnelling occurs, as observed, for example, in Ref. [6]. In Figure 4c–d, different coalescence mechanisms can be observed as functions of void distribution: the voids on the left, which are contained in the potential crack plane normal to the loading direction, coalesce via impingement, whilst the void at the right, which is oriented at ~45° with respect to the loading direction, coalesces with the crack via shear decohesion. This is consistent with the findings in Ref. [17]. In Figure 4d, shear fracture via a narrow band can be seen at the right. The voids contained in the crack are shallow, and some of them seem to have reoriented and flattened via the localized shear band deformation, as studied numerically in Ref. [20].

In Figure 4a–d the sample border can be seen. The grey value difference between the sample and the air is, however, lower than in the 2D sections shown in Figure 2. This is due to the low sensitivity of SRCL towards spatial frequencies approximatively parallel to the rotation axis but the relatively good sensitivity towards high spatial frequencies perpendicular to the axis. As a result, the high-frequency surface roughness of the specimen can be seen but not the strong contrast between the alloy matrix and the air. Some laminography artefacts starting from voids and oriented at ~65° with respect to the horizontal axis can be seen. These artefacts are intrinsic to the laminography technique [16]. They are, however, relatively weak, and in the present case do

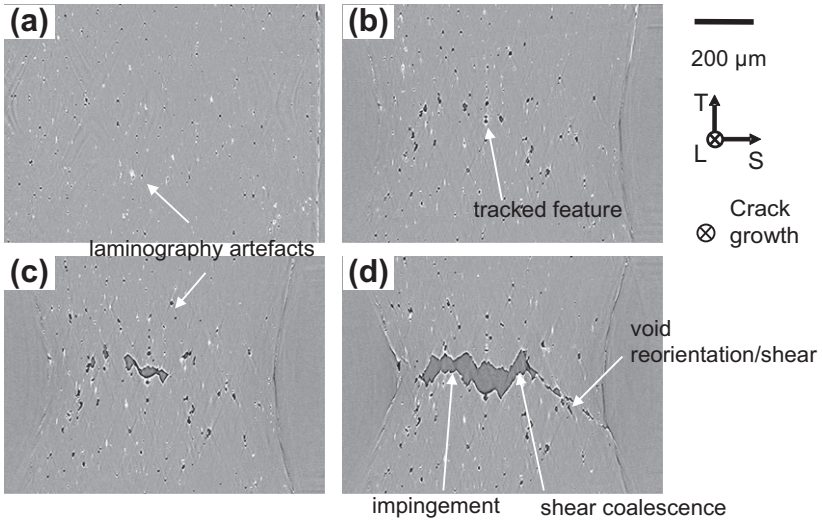

Figure 4. 2D sections of reconstructed SRCL data in the through-thickness plane at a distance of ~50 µm from the initial notch shown for different CMODs. (a) As-received material; (b) CMOD = 1.625 mm; (c) CMOD = 1.875 mm; (d) CMOD = 2.0625. Information on the supplementary loading steps is given in video 3.

not influence the damage segmentation through grey value thresholding. In cases where shear decohesion in narrow bands of similar orientation takes place between two voids, the artefact may make analysis of the mechanism more ambiguous.

In conclusion, in this experiment the feasibility of 3D in situ crack initiation and propagation in a relatively large aluminium sheet via SRCL has been shown. It provides unprecedented insights into damage mechanisms for sustained crack growth in an engineering-relevant sample geometry. Different mechanisms in void growth and shear coalescence mechanisms between crack initiation and propagation could be seen, which highlights the novel opportunities of SRCL with respect to SRCT, where only small specimens can be investigated in situ and only crack initiation with limited plastic zone sizes can be observed. The obtained in situ SRCL data now provide the opportunity to measure void growth as a function of strain and provide detailed comparisons for theoretical predictions. As such, models may be validated [21] and the potential arises to develop improved model formulations.

The authors would like to acknowledge Alcan CRV for technical discussion and materials supply. Andre Pineau and Jacques Besson are thanked for technical discussion.

Supplementary data associated with this article can be found, in the online version, at doi:10.1016/j.scriptamat.2011.09.005.

[1] W.M. Garrison, N.R. Moody, J. Phys. Chem. Solids 48 (1987) 1035–1074.
[2] J.C. Lautridou, A. Pineau, Eng. Fract. Mech. 15 (1981) 55–71.
[3] H. Toda, E. Maire, S. Yamauchi, H. Tsuruta, T. Hiramatsu, M. Kobayashi, Acta Mater. 59 (2011) 1995–2008.
[4] C. Landron, O. Bouaziz, E. Maire, J. Adrien, Scripta Mater. 63 (2010) 973–976.
[5] F. Bron, J. Besson, Eng. Fract. Mech. 73 (2006) 1531–1552.
[6] T.F. Morgeneyer, J. Besson, H. Proudhon, M.J. Starink, I. Sinclair, Acta Mater. 57 (2009) 3902–3915.
[7] T.F. Morgeneyer, M.J. Starink, I. Sinclair, Acta Mater. 56 (2008) 1671–1679.
[8] L. Helfen, A. Myagotin, P. Pernot, M. DiMichiel, P. Mikulík, A. Berthold, T. Baumbach, Nucl. Instrum. Methods Phys. Res. A 563 (2006) 163–166.
[9] F. Xu, L. Helfen, A.J. Moffat, G. Johnson, I. Sinclair, T. Baumbach, J. Synchrotron Radiat. 17 (2010) 222–226.
[10] A.J. Moffat, P. Wright, L. Helfen, T. Baumbach, G. Johnson, S.M. Spearing, I. Sinclair, Scripta Mater. 62 (2010) 97–100.
[11] L. Helfen, T. Baumbach, P. Mikulik, D. Kiel, P. Pernot, P. Cloetens, J. Baruchel, Appl. Phys. Lett. 86 (2005) 071915.
[12] L. Helfen, A. Myagotin, P. Mikulík, P. Pernot, A. Voropaev, M. Elyyan, M. Di Michiel, J. Baruchel, T. Baumbach, Rev. Sci. Instrum. 82 (2011) 063702.
[13] P. Cloetens, M. Pateyron-Salome, J.Y. Buffiere, G.J. Peix Baruchel, F. Peyrin, M. Schlenker, J. Appl. Phys. 81 (1997) 5878–5885.
[14] L. Helfen, T. Baumbach, P. Cloetens, J. Baruchel, Appl. Phys. Lett. 94 (2009) 104103.
[15] K. Krug, L. Porra, P. Coan, G. Tauber, A. Wallert, J. Dik, A. Coerdt, A. Bravin, M. Elyyan, L. Helfen, T. Baumbach, J. Synchrotron Radiat. 15 (2008) 55–61.
[16] L. Helfen, A. Myagotin, A. Rack, P. Pernot, P. Mikulik, M. Di Michiel, T. Baumbach, Phys. Stat. Sol. A 204 (2007) 2760–2765.
[17] A. Weck, D.S. Wilkinson, Acta Mater. 56 (2008) 1774–1784.
[18] M.H. Meliani, Z. Azaria, G. Pluvinage, Y.G. Matvienko, Eng. Fract. Mech. 77 (2010) 1682–1692.
[19] B. Tanguy, J. Besson, R. Piques, A. Pineau, Eng. Fract. Mech. 72 (2005) 49–72.
[20] I. Barsoum, J. Faleskog, Int. J. Solids Struct. 48 (2011) 925–938.
[21] T. Pardoen, F. Scheyvaerts, A. Simar, C. Tekoglu, P.R. Onck, C. R. Physique 11 (2010) 326–345.